Journal Pre-proof

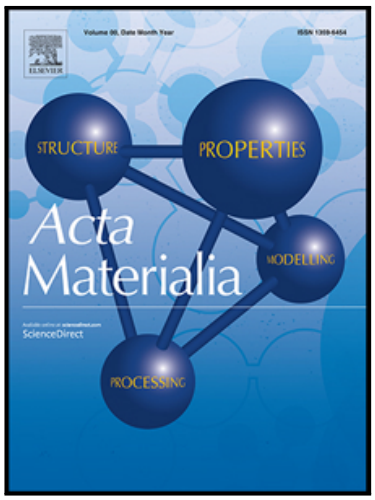

High-speed Synchrotron X-ray Imaging of Glass Foaming and Thermal Conductivity Simulation

Martin B. Østergaard , Manlin Zhang , Xiaomei Shen , Rasmus R. Petersen , Jakob König , Peter D. Lee , Yuanzheng Yue , Biao Cai

PII: S1359-6454(20)30173-7
DOI: https://doi.org/10.1016/j.actamat.2020.02.060
Reference: AM 15883

To appear in: *Acta Materialia*

Received date: 11 October 2019
Revised date: 24 January 2020
Accepted date: 26 February 2020

Please cite this article as: Martin B. Østergaard , Manlin Zhang , Xiaomei Shen , Rasmus R. Petersen , Jakob König , Peter D. Lee , Yuanzheng Yue , Biao Cai , High-speed Synchrotron X-ray Imaging of Glass Foaming and Thermal Conductivity Simulation, *Acta Materialia* (2020), doi: https://doi.org/10.1016/j.actamat.2020.02.060

High-speed Synchrotron X-ray Imaging of Glass Foaming and Thermal Conductivity Simulation

Martin B. Østergaard[1], Manlin Zhang[2], Xiaomei Shen[2], Rasmus R. Petersen[1], Jakob König[3], Peter D. Lee[4,5,*], Yuanzheng Yue[1,*], Biao Cai[2,*]

[1]Department of Chemistry and Bioscience, Aalborg University, DK-9220 Aalborg East, Denmark

[2]School of Metallurgy and Materials, University of Birmingham, Birmingham B15 2TT, UK

[3]Advanced Materials Department, Jožef Stefan Institute, SI-1000 Ljubljana, Slovenia

[4]Department of Mechanical Engineering, University College London, Torrington Place, London WC1E 7JE, UK

[5]Research Complex at Harwell, RAL, Didcot, OX11 0FA, UK

[*]Corresponding authors. E-mails: P.D.L. peter.lee@ucl.ac.uk, Y.-Z.Y. yy@bio.aau.dk, and B.C. b.cai@bham.ac.uk

Abstract

Glass foams are attractive thermal insulation materials, thus, the thermal conductivity (λ) is crucial for their performance. Understanding the foaming process is critical for process optimization. Here, we applied high-speed synchrotron X-ray tomography to investigate the change in pore structure during the foaming process, quantifying the foam structures and porosity dynamically. The results can provide guidance for the manufacturing of glass foams. The 3D pore structures were also used to computationally determine λ of glass foams. We used the simulated λ to develop a new analytical model to predict the porosity dependence of λ. The λ values predicted by the new model are in excellent agreement with the experimental data collected from the literature, with an average error of only 0.7%, which performs better than previously proposed models.

Keywords: Glass foam; Thermal conductivity; 3D image analysis; Simulation; Porosity

1. Introduction

Glass foams are attractive insulation materials as their high porosity results in a low thermal conductivity, thus, a good thermal insulation ability, in combination with load-bearing capability, resistance to humidity, very long lifespan, recyclability, and non-combustibility [1]. Capability to predict the thermal conductivity is important for assessing the insulating behavior of porous materials, e.g., glass foams. Focusing on glass foams, the thermal conductivity decreases roughly linearly with decreasing foam density, or increasing porosity [2–4]. As the porosity increases, the contributions of each phase and pore structure become increasingly important. The thermal conductivity of highly porous glass foams is, therefore, highly dependent on the contribution of the glass phase [5] and its susceptibility to crystallization or its crystal content from foaming residues [6,7], the composition of the gaseous phase in the pores [8], the porosity type (open or closed) and the pore structure (pore size and the thickness of the struts and walls) [2,3,7,9–11].

In order to obtain a high porosity, it is necessary to optimize the glass foaming process. The most common foaming method is a chemical approach, where glass powder is mixed with foaming agents that generate gas during heating, and the gas forms bubbles within the viscous glass [1]. *Ex situ* measurements have been used to determine foaming conditions such as the optimum heating rate [12–14], maximum foaming temperature [15–19], isothermal heating duration [2,13,20], and foaming agent content [21,22]. The drawback of these measurements is the inaccuracy in obtaining the optimum temperatures, for example the maximum foaming temperature is usually determined in steps of 25–50 °C. One *in situ* technique, hot stage microscopy that has been used to measure the change in the sample size as it expands during heating, has proved useful [23–27]. However, this technique only gives volumes, not providing any information on the pore structure.

X-ray tomography can provide three-dimensional information on the porous structure with high spatial resolution and quantitative structural details [3,10,17,28,29]. In these studies, analyses were carried out on glass foams after cooling, and thus, the dynamic changes in the porous structure were not revealed. Despite this limitation, new insights into the development of the structure were obtained by the *ex situ* tomography. Recently, changes in the macro- and microstructure have been monitored *in situ* in changing external conditions, e.g., during heating or pressing using high-speed synchrotron X-ray tomography, which here refers to capturing tomograms within seconds or sub-seconds. The technique has been used in monitoring liquid to solid transformations of metals [30,31], outgassing of volcanic glass [32], heating of dough during breadmaking [33], melting of waste glass [34], and foaming of metals [35].

In this study, cathode ray tube (CRT) panel glass is foamed using the mixture of manganese oxide and carbon as foaming agents in a proper viscosity window (10^4-10^6 Pa s) [36]. CRT glass is used for producing glass foams for the following reasons. First, CRT glass is landfilled, and thus can be recycled and reused, benefiting environment protection and cost reduction of raw materials. Second, it has a lower thermal conductivity than most of commercial glasses. Third, it does not crystallize during foaming, and this is advantageous for controlling foaming process and for suppressing thermal conductivity of final product. We use high-speed synchrotron X-ray tomography to obtain tomograms of a glass foam during the foaming process, and hence, dynamically monitor the expansion and evolution of the porous structure. Using this technique, we reconstruct the macroscopic structure of the glass foam at different temperatures and acquire the changes in pore size and porosity during heating. Image-based simulations of the macroscopic structure are used to determine the thermal conductivity of

the glass foams. This allows us to model the porosity dependence of the thermal conductivity of glass foams.

2. Experimental

2.1. Sample Preparation

Cathode ray tube (CRT) panel glass powder was mixed with 2.50 mol% carbon and 1.99 mol% Mn_3O_4 as described in Ref. [25]. A pellet of the powder mixture (13 mg) was uniaxially pressed by hand to form a cylinder with a diameter of 1 mm and the height of approx. 4 mm. The pellet was transferred to an alumina crucible that was inserted into a radiation furnace for foaming.

2.2 Foaming and *in situ* tomography

A bespoke PID-controlled resistance furnace measuring the temperature just below the sample (described in Ref. [37]) was used at beamline I12 (Diamond Light Source, United Kingdom) to perform *in situ* synchrotron tomographic foaming experiments. The sample was rapidly heated to 585 °C and further heated to 840 °C at 5 °C min^{-1}. Before heating, the chamber was flushed with nitrogen, and a constant nitrogen flow (approx. 5 mL min^{-1}) was introduced during heating to ensure an inert atmosphere. A 53 keV monochromatic X-ray beam was used, and the radiographs were acquired using a PCO.edge camera at camera module 3 [38]. High speed tomographic scans were carried out when the sample was continuously rotating during heating. One 3D dataset with 1000 radiographs were obtained in intervals of 5 s over an angle of 180°. The downloading of the 3D data was completed within the next 5 s when the sample rotated another 180°. Hence, the cycle time was 10 s.

2.3 Image analysis

The radiographs were utilized to reconstruct the structure of the glass foam during heating with a voxel size of 3.24 µm voxel^{-1}. The images were processed and analyzed using Avizo and ImageJ softwares. To ensure identical procedure for segmentation of all images, we applied a machine-learning-based image processing plug-in in ImageJ (Trainable Weka Segmentation [39]). Pixels were manually assigned to a distinct phase (solid or gas), through the trainable Weka Segmentation, creating a model (or classifier) that was then applied to all images. The porosity was determined as the ratio between the volume of pores and the total volume. The pore thickness (a measure of the pore diameter) at different temperatures during heating was evaluated using the BoneJ plug-in [40] in ImageJ. The experiment was performed three times to ensure reproducibility.

2.4 Simulation of the thermal conductivity

The thermal conductivity experiment simulation built-in module in the Avizo software was used to perform the image-based simulation of the thermal conductivity (λ). The module uses the result of the segmentation to rum image-based thermal simulation solving the Fourier's law. The 3D pore structure after segmentation was used for the 3D image-based thermal simulation. A representative 3D volume of 1620 × 1620 x 1620 µm was imported to Avizo for use in simulation. The heat flow was from the top face of the volume with input temperatures of 373 K to the bottom face with output temperature of 298 K. Three series of simulations were carried out: the first series considers only the glass phase as the gas phase is considered non-conducting (i.e. λ_g = 0 W m^{-1} K^{-1}), whereas the second and third series consider both the glass and the gas phases conducting with the gas phase being either air or CO_2. The λ of the solid glass (λ_s) was set to 0.925 W m^{-1} K^{-1} [2] (as calculated by the Choudhary and Potter model [41]). The thermal conductivity of the gas was set to 0.026 W m^{-1} K^{-1} for air gas phase [42] and 0.016

W m^{-1} K^{-1} for CO_2 gas phase [43], respectively. The simulation was performed on 3D volumes at different heating temperatures hence different porosities.

3. Results and discussion

3.1. Quantification of the foaming process

The reconstructions of the glass foams at different temperatures during heating show significant changes in the porous structure (Fig. 1). At 776 °C, a nearly pore free sample is shown with only minor degree of pores, but with increasing temperature, the number of pores increases until a temperature around 803 °C is reached. Further heating up to 835 °C leads to a gradual increase in the pore size. The foaming process during heating can be observed in the supplementary movie 1. The change in the measured pore size is shown in Fig. 2. The significant increase in the porosity at temperatures below 800 °C (porosity increases from 5 to 60 %) is in major part caused by nucleation of new pores, as their size does not change significantly (Fig. 2). The increases of the number of pores can be observed in Figs. 1a to 1c. This mechanism was recently observed in foaming of metals [35]. Recently it was observed in glass foam light-weight aggregates that the porosity increases without any change in pore size before reaching a porosity around 60 % [11]. The higher porosities at the later stage of the heating is thereafter caused by an increase in the pore size. The porosity increase is also visualized in the reconstructed 3D structures in Fig. 3a-c and 2D slices in Fig. 3d-f, where the brightness increases due to the larger pore size. The increase in the pore size above 800 °C results in a further increase in the porosity (from 60 to 90 %) owing to the following factors. Firstly, the pressure inside the pores is higher than that in the atmosphere due to the gases evolved by the foaming agent, and hence, the melt expands. As the oxidization of the carbon and the reduction of the manganese progress, more gas is

evolved, leading to a larger expansion [24]. At the same time, increasing temperature lowers the melt viscosity, thus decreasing the opposing force for the expansion of the pores. Secondly, the initial pores are mainly spherical [18] which minimizes the surface energy. However, as the melt viscosity decreases, the pore walls become thinner and eventually break, triggering the coalescence process or coarsening phenomena that increases the pore size and creates non-spherical pores [44]. The coalescence also provokes incorporation of small pores into large pores, and thereby the small pores disappear [45]. The non-spherical shape of the pores enhances the pore coalescence [46]. The non-spherical pores should transform into a sphere to minimize surface tension, but there is not sufficient time available as pore walls continuously break and small pores diffuse into the larger pores, thus, the pore shape remains polyhedral. Fig. 4 shows how two non-spherical large pores combine into one due to the rupture of the pore wall.

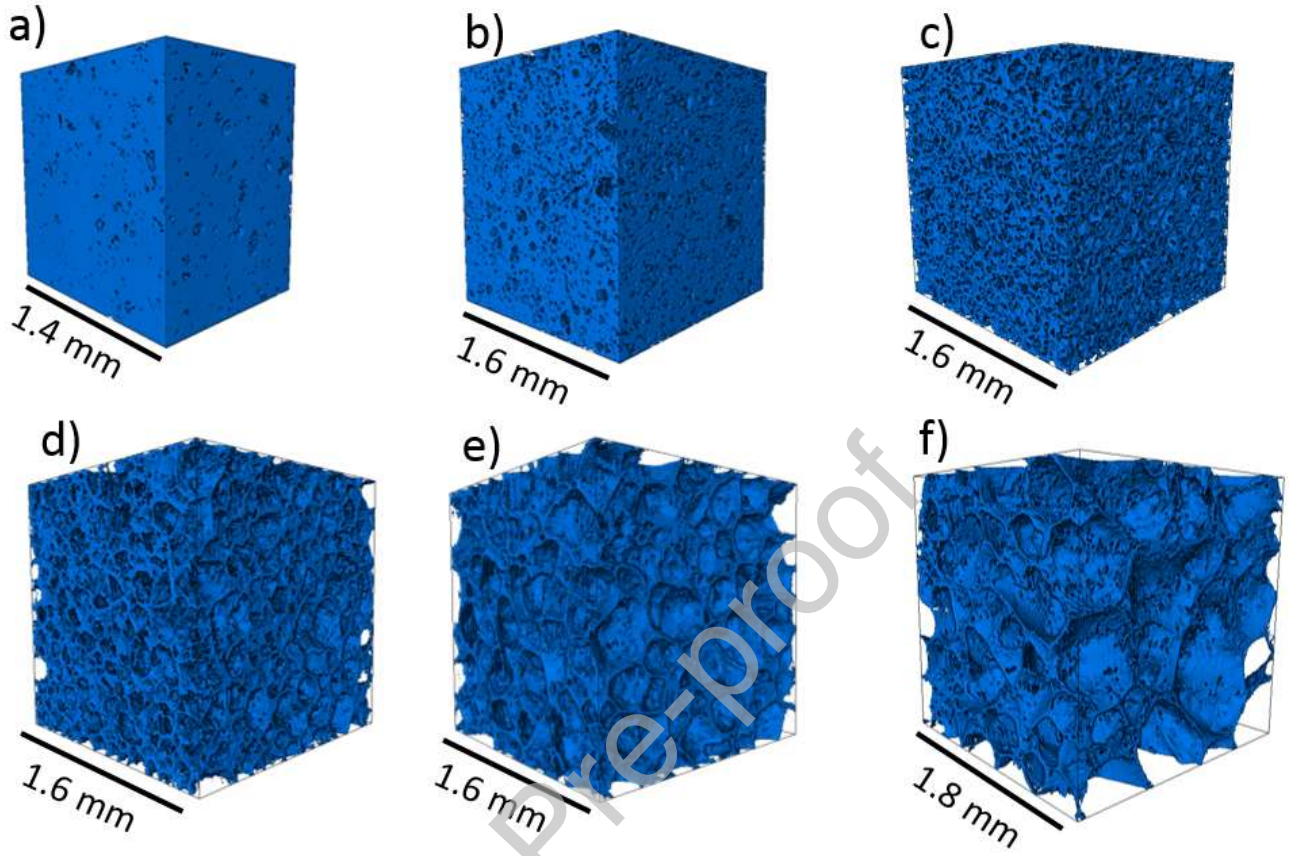

Fig. 1. 3D rendering of glass foams (blue refers to the glass and the empty places in the image are porosities) at different temperatures during heating, a) 776 °C, b) 787 °C, c) 803 °C, d) 811 °C, e) 819 °C, and f) 835 °C.

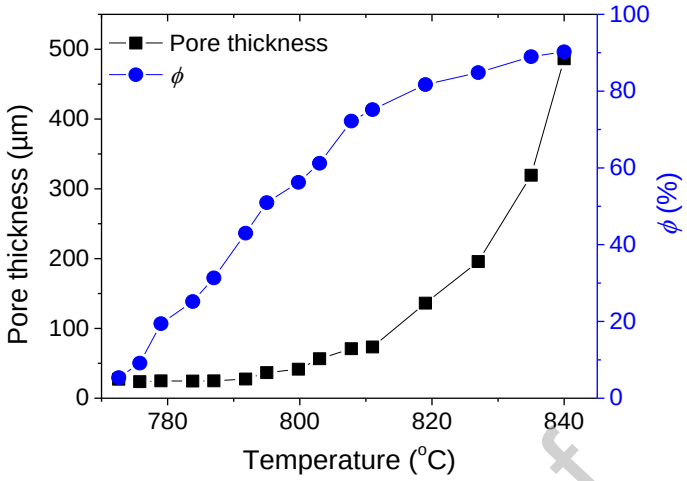

Fig. 2. Changes of the average pore thickness and porosity (ϕ) during heating. The thickness measurements were performed three times.

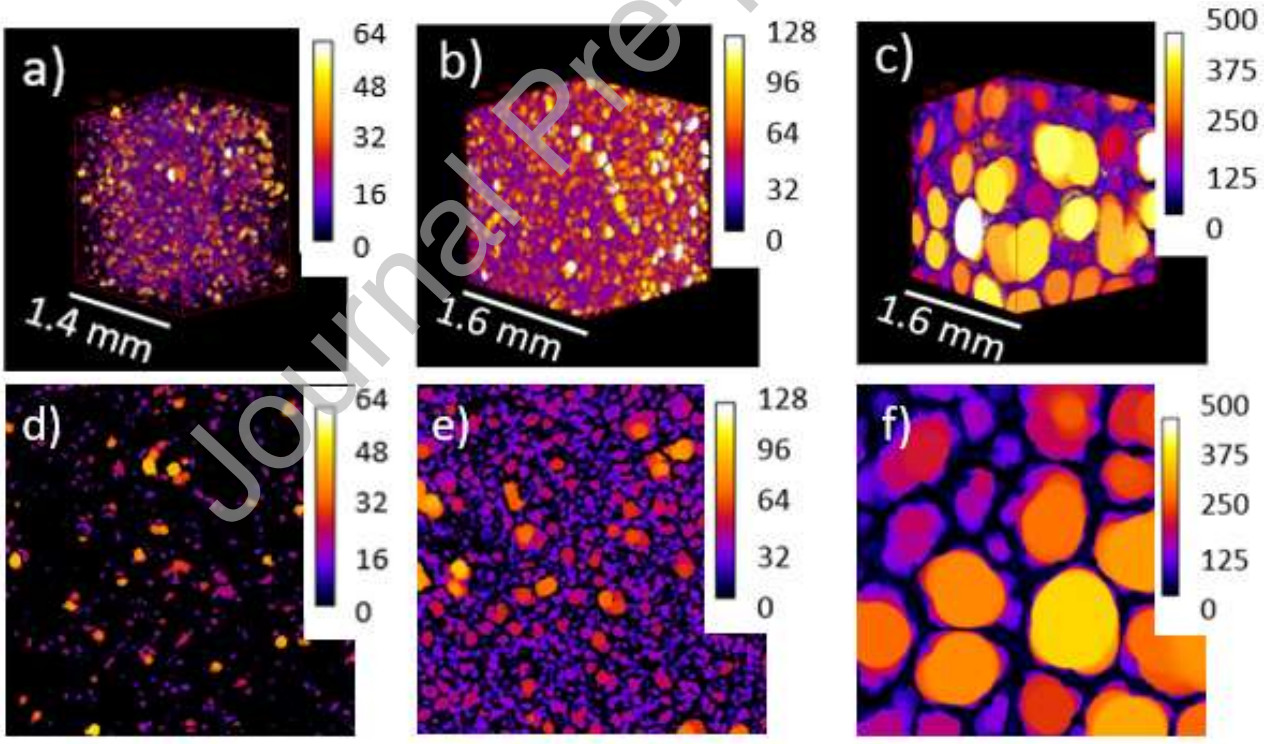

Fig. 3. 3D (a-c) and 2D (d-f) rendering of the thickness of the pores showing the changing pore size with increasing temperature at a) and d) 776 °C, b) and e) 800 °C, and c) and f) 827 °C. The color scale shows the pore thickness in µm.

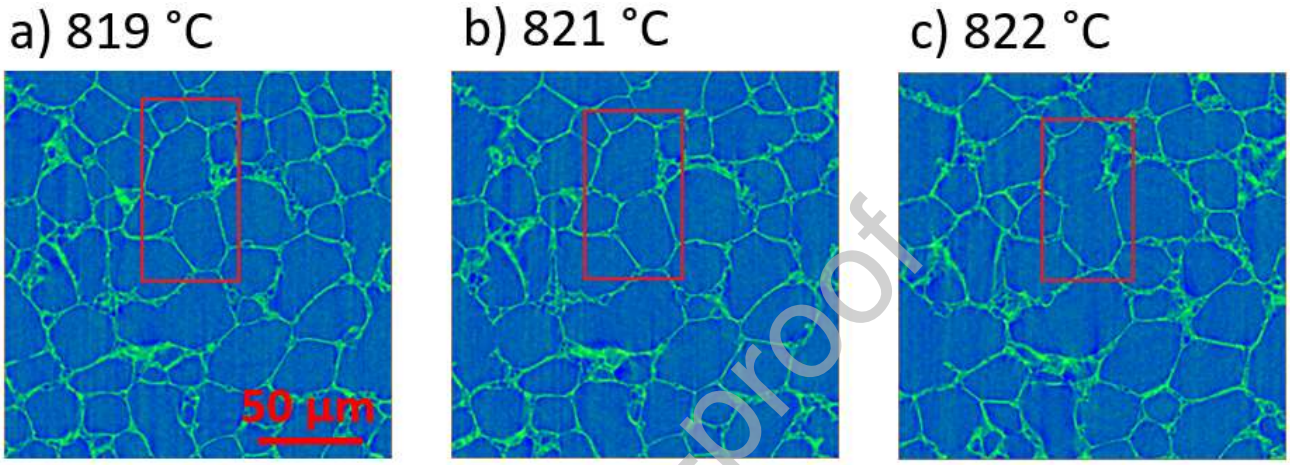

Fig. 4. Coalescence of the pores during heating (marked with a rectangle): a) two pores separated by a pore wall, b) beginning of the rupture in the pore wall, and c) complete rupture of the pore wall, forming a combined larger pore with irregular shape. Scalebar is shown in a) and is valid for all images.

3.2. Image-based simulation of the thermal conductivity

The heat gradient through the reconstructed glass foam is visualized in Fig. 5. Based on the heat gradients, the porosity dependence of the thermal conductivity (λ) is simulated using image-based simulation for glass foams based on the 3D pore structures (Fig.6). When considering the gas phase as non-conducting, the heat is only transported through the glass phase (Fig. 5a), whereas when considering the actual gas phase the heat is transported through both gas and solid phases (Fig. 5b). Hence, the glass skeleton is only visible in the simulation when the pores are considered non-

conducting. Simulations of λ throughout the porosity range of 5–90 % are carried out for the three cases taking into consideration the different gaseous contributions, i.e., 0, 0.016, and 0.026 W m^{-1} K^{-1} for the thermal insulator, CO_2, and air, respectively (Fig. 6). We note, that the pore structure changes as the porosity increases. The thermal conductivity of the solid phase (λ_s) is 0.925 W m^{-1} K^{-1} [2]. The gaseous contribution is insignificant at low porosity as the dominant phase in the sample is glass with two orders of magnitude higher thermal conductivity. However, with increasing porosity, the difference in λ gets more pronounced, displaying an increase in λ in the order of air > CO_2 > insulating, agreeing with previous experimental findings [8]. This indicates the importance of considering the gas phase contribution into simulations.

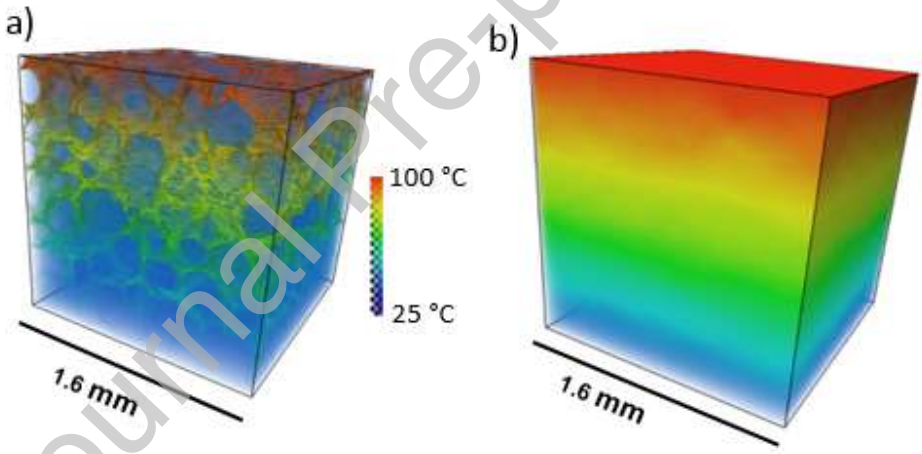

Fig. 5. Simulated temperature gradient through a glass foam with a) the gas phase considered an insulator and b) the gas phase included as air.

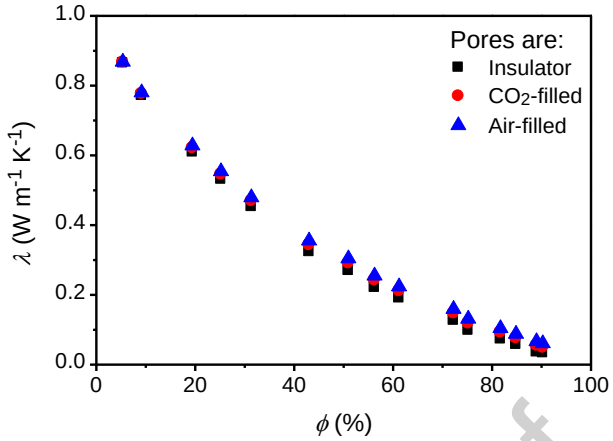

Fig. 6. Simulation of the thermal conductivity (λ) as a function of porosity (ϕ) and gas phase for glass foams with glass a conductivity of 0.925 W m^{-1} K^{-1} and pores as thermal insulator or pores filled with CO_2 or air.

The simulated λ values at different porosities are compared to reported experimental values for the glass foams derived from CRT panel glass [2,5,8,10,20,22,47] in Fig. 7. We note that in the literature the porosities in some cases are not reported, and we therefore calculate it using the reported bulk/powder density values or using a powder density (ρ_s) of 2.76 g cm^{-3} [24]. As expected the simulated curves for real gas phases (CO_2 or air) describe the experimental values better than the simulated curve, where the gas phase is assumed to be a thermal insulator, since in the real samples CO_2, O_2, CO, Ar, and/or N_2 are present in the pores. These data clearly show that the gas phase composition is a crucial parameter for simulating λ at high porosities. Some reported values are higher than the simulated values, which is very likely linked to a higher solid contribution due to crystal residues from foaming agents in the solid phase [6] or a difference in the pore structure, e.g., in pore size [9–11]. Both differences increase the contribution of the solid phase to the effective thermal

conductivity. The simulated λ is roughly linearly decreasing with the porosity in the porosity range 55–90 % (Fig. 7). A deviation from the general trend is seen at a porosity ~73 %. This is plausibly due to changes in the porous structure, as it appears in the same porosity range where the pore size starts to increase (Fig. 2).

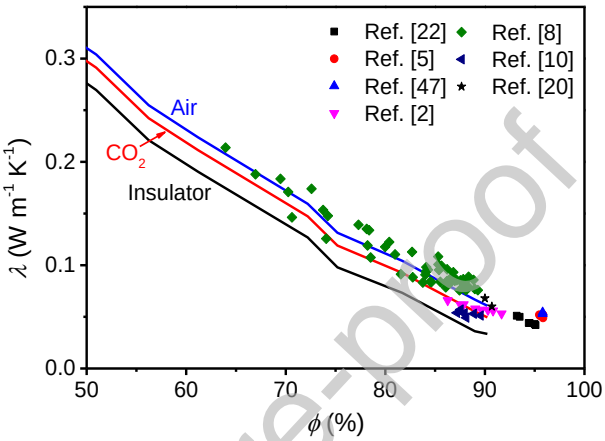

Fig. 7. Comparison of the simulated thermal conductivity (λ) and experimental λ values in glass foams based on CRT panel glass from the literature.

3.3. Modeling the porosity dependence of the thermal conductivity

The simulated λ values are in good agreement with the experimental ones from the literature when exceeding a porosity of 60 % (Fig. 7). Due to a lack of data for the lower porosity region, we fit a linear equation to the simulated values for porosities of above 43 %. The fit is performed for the case of CO_2-filled pores. The porosity dependence of λ can thus be expressed as Eq. 1:

$$\lambda = -0.01 + (1 - \phi)0.60 \quad (1)$$

Considering the λ-values of the solid (0.925 W m^{-1} K^{-1}) and gas phase (0.016 W m^{-1} K^{-1}), Eq. 1 can be converted to Eq. 2.

$$\lambda = \lambda_g(\phi - 1) + \frac{2}{3}(1 - \phi)\lambda_s \quad (2)$$

where λ, λ_g, and λ_s is the thermal conductivities of the foam, the gas, and the solid, respectively, and ϕ is the porosity of the glass foam. The model is limited within a porosity range of 40–95 %. Additionally, the influence of pore size was not investigated, but it is anticipated that the model behaves well for pore sizes >0.1 µm (Knudsen effect) and <4 mm (convective contribution). The Knudsen effect results in significantly lower thermal conductivity, while the convective contribution leads to higher thermal conductivity of porous materials.

To compare Eq. 2 with the existing models regarding the prediction quality of the porosity dependent λ value for porous materials, we test four other analytical models which have been widely used to simulate the thermal conductivity, namely, the Russell (Eq. 3) [48], the Landauer (Eq. 4) [49], the Schuetz-Glicksman (Eqs. 5 and 6) [50], and the Doherty-Hurd-Lestor (Eq. 7) [51] models, against the simulated λ values (Fig. 8). We note that many more models exist based on theoretical or semi-empirical work [52]. The Russell model works well for kaolin-based foams and calcium aluminate foams with porosity > 65 % [53], while the Landauer model works well in open porous (< 65 %) materials such as tin oxide, alumina, and zirconia ceramics [53]. Both the Schuetz-Glicksman and Doherty-Hurd-Lestor models work on highly porous polymeric foams [52].

$$\lambda = \frac{\lambda_s(\lambda_s + \phi^{\frac{2}{3}}(\lambda_g - \lambda_s))}{\lambda_s + (\lambda_g - \lambda_s)(\phi^{\frac{2}{3}} - \phi)} \quad (3)$$

where λ_s and λ_g are the solid and gas conductivity, respectively, and ϕ is the porosity.

$$\lambda = \frac{1}{4}[(\lambda_g(3\phi - 1)) + \lambda_s(3\phi_s - 1) + ([\lambda_g(3\phi - 1) + \lambda_s(3\phi_s - 1)]^2 + 8\lambda_s\lambda_g)^{½}] \quad (4)$$

where ϕ_s is the solidity, i.e., fraction of the solid in the foam (ϕ_s=1− ϕ).

$$\lambda = \lambda_g + K(1 - \phi)\lambda_s \quad (5)$$

$$K = \tau(\frac{2}{3} - \frac{f_s}{3}) \quad (6)$$

where τ is the tortuosity factor and f_s is the fraction of the solid located in the struts. The *K*-factor was estimated to be close to 0.34 for glass foams prepared from CRT panel glass and MnO_2 by treating the *K*-factor as a fitting parameter [2].

$$\lambda = \lambda_g + \frac{2}{3}(1 - \phi)\lambda_s \quad (7)$$

Among these models, the Schuetz-Glicksman (Eq. 5) [50] and the Doherty-Hurd-Lestor (Eq. 7) [51] models are the same when K = 2/3 in the Schuetz-Glicksman expression. Both Eq. 5 and Eq. 7 are similar expressions to Eq. 2, yet different from Eq. 2, in which we account for the porosity in both the first and second terms in contrast to the previous models. These four models are, as Eq. 2, based on the porosity and the conductions of the solid and the gas phase. All models treat the conduction through solid (λ_s) and gas (λ_g) as decoupled. We use the same values for λ_s and λ_g as described earlier (λ_s=0.925 W m^{-1} K^{-1} and λ_g=0.016 W m^{-1} K^{-1}). In other words, we assume there is pure CO_2 in the pores and the solid matrix composes of CRT panel glass, where the solid conduction, i.e. λ_s=0.925 W m^{-1} K^{-1}, is calculated based on a model developed by Choudhary and Potter [41]. The λ_s of a glass obtained by remelting CRT panel glass is measured to be 0.866 W m^{-1} K^{-1}, while that of a CRT panel

glass remelted with 4 wt% MnO_2 is 0.932 W m^{-1} K^{-1} [6]. Therefore, the calculated λ of the solid phase (λ_s=0.925 W m^{-1} K^{-1}) already includes the contributions from the incorporation of manganese oxide into the glass phase and a low degree of Mn_3O_4 or MnO crystal residues in the glass matrix [2].

The simulated λ is well described by the Landauer model for porosities <40 % and by the new model (Eq. 2) for porosities >40 % (Fig. 8a). Glass foams for insulating purposes are highly porous and therefore, the new model is promising. This is supported by Fig. 8b, showing that the new model (Eq. 2) depicts the λ trend much better than the four other models.

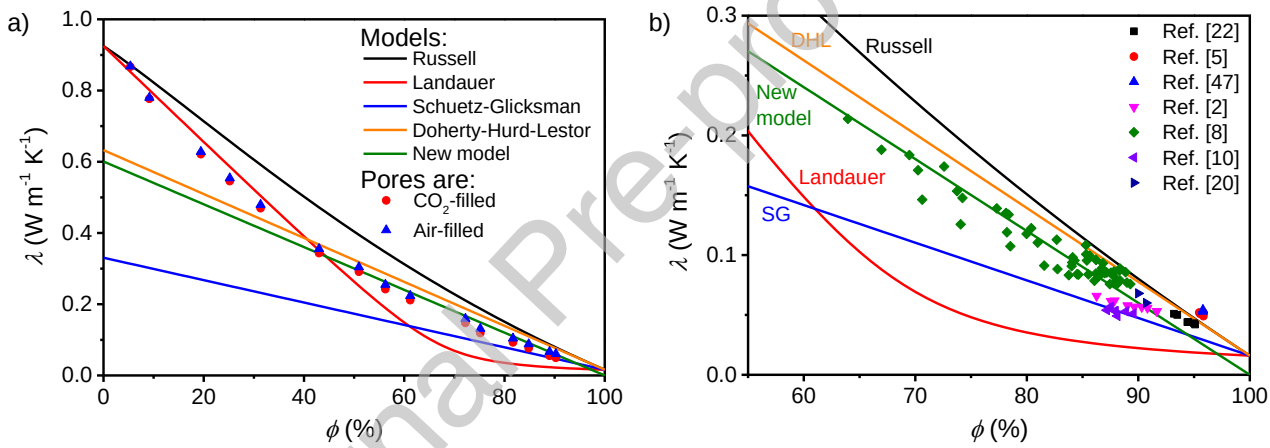

Fig. 8. Comparison of the ability of five models (Russell, the Landauer, the Schuetz-Glicksman (SG), Doherty-Hurd-Lestor (DHL), and the new model (Eq. 2)) to describe the simulated thermal conductivity (λ) based on the porosity (ϕ) (a) and the experimental λ data of glass foams based on CRT panel glass from various studies (b) (see labels). The λ values used in the models for solid and gas are 0.925 W m^{-1} K^{-1} and 0.016 W m^{-1} K^{-1}, respectively.

Glass foams based on CRT panel glass were used for the initial comparison of the models since these are similar to the simulated glass foams. To make a broader comparison of the models, we model

the ϕ dependence of λ for glass foams based on different types of glasses and containing different gases and compare them with their experimental λ values from the literature (Fig. 9a). The comparison was made for the porosity >40 %. Experimental λ data are taken from Refs. [2,3,54–57,4,5,8,10,20,22,27,47], and the average difference between the modeled and experimental values is shown in Fig. 9b. In order to model the ϕ dependence of λ, we have made the following assumptions regarding λ_s and λ_g. The λ_s contributions of CRT panel glass, funnel glass, and soda-lime silica glasses (window, flat, bottle) are 0.925 [2], 1.046 [58], and 1.1 W m^{-1} K^{-1} [3], respectively. For glass mixtures, we presume a linear relation between the λ_s and the fraction of the specific glass, and thereby calculate the approximate λ_s. λ_g of CO_2, O_2, N_2, Ar (mixture with CO_2), N_2 (mixture with CO_2), H_2O, and SO_2 are 0.016 [43], 0.026 [42], 0.026 [42], 0.016 [8], 0.023 [8], 0.019 [59], and 0.0099 W m^{-1} K^{-1} [60], respectively. The gas might be a multicomponent phase as reported previously [5,8], but to predict λ, we assume one-phase gas compositions unless λ_g of the multicomponent gas phase is reported. For simplicity, we do not consider the ratio of the closed and the open pores in modeling, but assume 100 % closed pores filled with the gas evolved during foaming, e.g., CO_2 released from carbonaceous substances, N_2 from TiN, and O_2 from MnO_2. In the case of a lack of porosity data, we acquire data by calculations based on the foam density and bulk solid density, where the solid density is 2.76 [8], 3.00 [61], and 2.48 g cm^{-3} [36] for CRT panel glass, CRT funnel glass, and soda-lime silica glasses, respectively.

To illustrate the difference between the new model (Eq. 2) and the four existing models analyzed in this paper, we plot the difference in the experimental and the modeled λ data against ϕ (Fig. 9). Eq. 2 is, in general, closer to the experimental values (Fig. 9a). In contrast, the Russell model underestimates,

whereas the Landauer and Schuetz-Glicksman models overestimate λ. Eq. 8 describes the difference between the modeled (λ_{model}) and the experimental (λ_{exp}) thermal conductivity values.

$$Difference = \frac{\lambda_{exp} - \lambda_{model}}{\lambda_{exp}} \cdot 100 \quad (8)$$

The average difference between the modeled and the experimental λ values, calculated for all the data, implies that the Russell model overestimates λ by 31 % (as the experimental value is 31 % lower than the predicted) and the Doherty-Hurd-Lestor overestimates by 24 %, while both the Landauer model and the Schuetz-Glicksman models underestimate λ by 60 % and 26 %, respectively. In contrast, the new model only exhibits a difference of 0.7 % on average for glass foams with porosity >40 % (Fig. 9b). The comparison suggests that Eq. 2 performs better than other models in terms of prediction of λ of glass foams.

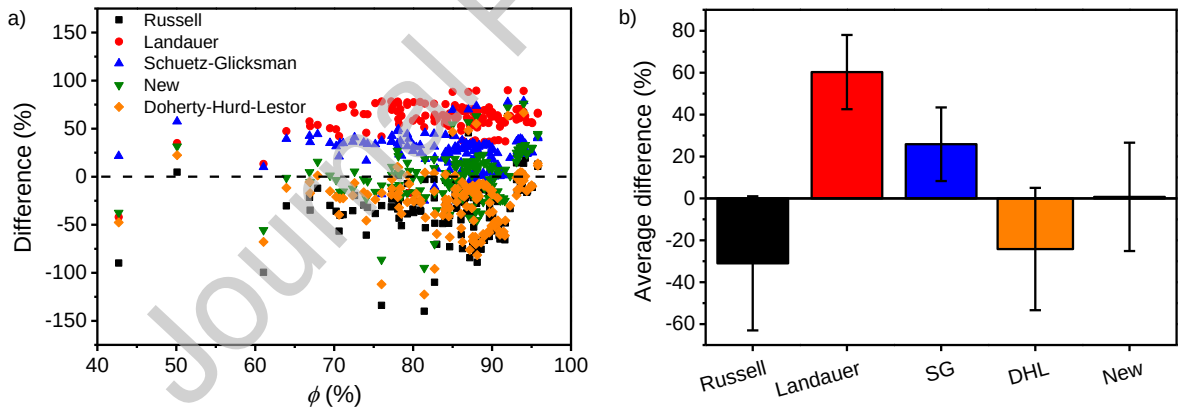

Fig. 9. a) Difference (Eq. 8) in the thermal conductivity (λ) between experimental values and those obtained through different models at different porosities (ϕ) for various types of glasses including, e.g., CRT and window glasses; b) Average difference in thermal conductivity for the Russell, Landauer, Schuetz-Glicksman (SG), Doherty-Hurd-Lestor (DHL), and new (Eq. 2) models.

4. Conclusions

The foaming of a glass melt is monitored using synchrotron X-ray tomography. The developing and growing pores cause an increase in the sample volume due to the gas formation, thus, the porosity of the sample increases. The initial increase in the porosity is caused by the formation of new small pores, while at higher temperatures the pores start to expand due to increasing internal pressure and decreasing viscosity. The highest porosity determined for the investigated glass foam is 90.2 %. Based on the 3D reconstructions of the glass foam structures at different temperatures, image-based simulations of the glass foam structures are used to determine the thermal conductivity (λ). The simulated λ decreases with increasing porosity and with a decreasing gas conduction.

Finally, we propose a new empirical model (Eq. 2) to effectively describe the porosity dependence of λ of glass foams (and plausibly other porous materials) as a function of porosity for the case of ϕ >40 %. The new model exhibits an average difference of only 0.7 % between the modeled and experimentally obtained λ values, compared to the average difference of 26–60 % achieved by the four considered analytical models.

Acknowledgements

M.B.Ø., R.R.P., J.K., and Y.-Z.Y. thank the Energy Technology Development and Demonstration Program (EUDP) for financial support under grant number 64015-0018. B.C. and P.D.L. acknowledge support provided by the Research Complex at Harwell, funded in part by EPSRC (EP/K007734/1, EP/P006566/1, and EP/L018705/1). B.C. acknowledges support through the Diamond Birmingham Collaboration funded by the University of Birmingham and the Alan Turing Fellowship. P.D.L

acknowledge support from the Royal Academy of Engineering Chair in Emerging Technologies. We gratefully acknowledge the Diamond Light Source, UK, for beamtime EE16188/1 at beamline I12.

Declaration of Competing Interest

The authors declare that they have no known competing financial interests or personal relationships that could have appeared to influence the work reported in this paper.

References

[1] G. Scarinci, G. Brusatin, E. Bernardo, Glass foams, in: M. Scheffler, P. Colombo (Eds.), Cell. Ceram. Struct. Manuf. Prop. Appl., Wiley-VCH Verlag GmbH & Co KGaA, Weinheim, 2005: pp. 158–176.

[2] R.R. Petersen, J. König, Y. Yue, The mechanism of foaming and thermal conductivity of glasses foamed with MnO_2, J. Non. Cryst. Solids. 425 (2015) 74–82.

[3] J.P. Wu, A.R. Boccaccini, P.D. Lee, R.D. Rawlings, Thermal and mechanical properties of a foamed glass-ceramic material produced from silicate wastes, Proc. Eighth Eur. Soc. Glas. Sci. Technol. Conf. Glas. Technol. Eur. J. Glas. Sci. Technol. A. 48 (2007) 133–141.

[4] F. Méar, P. Yot, R. Viennois, M. Ribes, Mechanical behaviour and thermal and electrical properties of foam glass, Ceram. Int. 33 (2007) 543–550.

[5] J. König, R.R. Petersen, N. Iversen, Y. Yue, Suppressing the effect of cullet composition on the formation and properties of foamed glass, Ceram. Int. 44 (2018) 11143–11150.

[6] M.B. Østergaard, R.R. Petersen, J. König, H. Johra, Y. Yue, Influence of foaming agents on thermal conductivity of the CRT panel glass, J. Non. Cryst. Solids. 465 (2017) 59–64.

[7] Y.A. Spiridonov, L.A. Orlova, Problems of foam glass production, Glas. Ceram. 60 (2003) 313–315.

[8] M.B. Østergaard, R.R. Petersen, J. König, M. Bockowski, Y. Yue, Impact of gas composition on thermal conductivity of glass foams prepared via high-pressure sintering, J. Non-Crystalline Solids X. 1 (2019) 100014.

[9] S. Köse, G. Bayer, Schaumbildung im system altglas-SiC und die eigenschaften derartiger schaumgläser, Glas. Ber. 55 (1982) 151–160.

[10] M.B. Østergaard, B. Cai, R.R. Petersen, J. König, P.D. Lee, Y. Yue, Impact of pore size on thermal conductivity of glass foams, Mater. Lett. 250 (2019) 72–74.

[11] C. Arriagada, I. Navarrete, M. Lopez, Understanding the effect of porosity on the mechanical and thermal performance of glass foam lightweight aggregates and the influence of production factors, Constr. Build. Mater. 228 (2019) 116746.

[12] A. Pokorny, J. Vicenzi, C. Pérez Bergmann, Influence of heating rate on the microstructure of glass foams., Waste Manag. Res. 29 (2011) 172–179.

[13] L. Lakov, K. Toncheva, A. Staneva, Z. Ilcheva, T. Simeonova, Composition , Synthesis and Properties of Color Architecture Building Foam Glass Obtained From Waste Packing Glass, J. Chem. Technol. Metall. 48 (2013) 125–129.

[14] B. Cicek, L. Esposito, A. Tucci, E. Bernardo, A.R. Boccaccini, P.A. Bingham, Microporous

glass ceramics from combination of silicate , borate and phosphate wastes, Adv. Appl. Ceram. 111 (2012) 415–422.

[15] A.S. Llaudis, M.J.O. Tari, F.J.G. Ten, E. Bernardo, P. Colombo, Foaming of flat glass cullet using Si_3N_4 and MnO_2 powders, Ceram. Int. 35 (2009) 1953–1959.

[16] V. Ducman, M. Kovacevic, The foaming of waste glass, Key Eng. Mater. 132–136 (1997) 2264–2267.

[17] J.P. Wu, A.R. Boccaccini, P.D. Lee, M.J. Kershaw, R.D. Rawlings, Glass ceramic foams from coal ash and waste glass : production and characterisation, Adv. Appl. Ceram. 105 (2006) 32–39.

[18] R. Taurino, I. Lancellotti, L. Barbieri, C. Leonelli, Glass-ceramic foams from borosilicate glass waste, Int. J. Appl. Glas. Sci. 5 (2014) 136–145.

[19] H.R. Fernandes, F. Andreola, L. Barbieri, I. Lancellotti, M.J. Pascual, J.M.F. Ferreira, The use of egg shells to produce Cathode Ray Tube (CRT) glass foams, Ceram. Int. 39 (2013) 9071–9078.

[20] E. Bernardo, F. Albertini, Glass foams from dismantled cathode ray tubes, Ceram. Int. 32 (2006) 603–608.

[21] V. Laur, R. Benzerga, R. Lebullenger, L. Le Gendre, G. Lanoë, A. Sharaiha, P. Queffelec, Green foams for microwave absorbing applications: Synthesis and characterization, Mater. Res. Bull. 96 (2017) 100–106.

[22] J. König, R.R. Petersen, Y. Yue, Fabrication of highly insulating foam glass made from CRT panel glass, Ceram. Int. 41 (2015) 9793–9800.

[23] R.R. Petersen, J. König, Y. Yue, Evaluation of foaming behavior of glass melts by high-temperature microscopy, Int. J. Appl. Glas. Sci. 7 (2016) 524–531.

[24] M.B. Østergaard, R.R. Petersen, J. König, M. Bockowski, Y. Yue, Foam glass obtained through high-pressure sintering, J. Am. Ceram. Soc. 101 (2018) 3917–3923.

[25] M.B. Østergaard, R.R. Petersen, J. König, Y. Yue, Effect of alkali phosphate content on foaming of CRT panel glass using Mn_3O_4 and carbon as foaming agents, J. Non. Cryst. Solids. 482 (2018) 217–222.

[26] H.R. Fernandes, D.D. Ferreira, F. Andreola, I. Lancellotti, L. Barbieri, J.M.F. Ferreira, Environmental friendly management of CRT glass by foaming with waste egg shells, calcite or dolomite, Ceram. Int. 40 (2014) 13371–13379.

[27] D. Hesky, C.G. Aneziris, U. Groß, A. Horn, Water and waterglass mixtures for foam glass production, Ceram. Int. 41 (2015) 12604–12613.

[28] L. Korat, V. Ducman, A. Legat, B. Mirtič, Characterisation of the pore-forming process in lightweight aggregate based on silica sludge by means of X-ray micro-tomography (micro-CT) and mercury intrusion porosimetry (MIP), Ceram. Int. 39 (2013) 6997–7005.

[29] V. Ducman, L. Korat, A. Legat, B. Mirtič, X-ray micro-tomography investigation of the foaming process in the system of waste glass-silica mud-MnO_2, Mater. Charact. 86 (2013) 316–321.

[30] M.A. Azeem, P.D. Lee, A.B. Phillion, S. Karagadde, P. Rockett, R.C. Atwood, L. Courtois, K.M. Rahman, D. Dye, Revealing dendritic pattern formation in Ni, Fe and Co alloys using synchrotron tomography, Acta Mater. 128 (2017) 241–248.

[31] C.L.A. Leung, S. Marussi, R.C. Atwood, M. Towrie, P.J. Withers, P.D. Lee, In situ X-ray imaging of defect and molten pool dynamics in laser additive manufacturing, Nat. Commun. 9 (2018) 1–9.

[32] F.W. von Aulock, B.M. Kennedy, A. Maksimenko, F.B. Wadsworth, Y. Lavallée, Outgassing from Open and Closed Magma Foams, Front. Earth Sci. 5 (2017) 1–7.

[33] P. Babin, G. Della Valle, H. Chiron, P. Cloetens, J. Hoszowska, P. Pernot, A.L. Réguerre, L. Salvo, R. Dendievel, Fast X-ray tomography analysis of bubble growth and foam setting during breadmaking, J. Cereal Sci. 43 (2006) 393–397.

[34] A.S. Choi, D.H. Miller, D.M. Immel, F.G. Smith, Investigation of high-level waste glass melting using X-ray computed tomography, Int. J. Appl. Glas. Sci. 8 (2017) 165–176.

[35] F. García-moreno, P.H. Kamm, T.R. Neu, F. Bülk, R. Mokso, C.M. Schlepütz, M. Stampanoni, J. Banhart, Using X-ray tomoscopy to explore the dynamics of foaming metal, Nat. Commun. 10 (2019) 1–9.

[36] R.R. Petersen, J. König, Y. Yue, The viscosity window of the silicate glass foam production, J. Non. Cryst. Solids. 456 (2017) 49–54.

[37] B. Cai, S. Karagadde, L. Yuan, T.J. Marrow, T. Connolley, P.D. Lee, In situ synchrotron tomographic quantification of granular and intragranular deformation during semi-solid compression of an equiaxed dendritic Al-Cu alloy, Acta Mater. 76 (2014) 371–380.

[38] M. Drakopoulos, T. Connolley, C. Reinhard, R. Atwood, O. Magdysyuk, N. Vo, M. Hart, L. Connor, B. Humphreys, G. Howell, S. Davies, T. Hill, G. Wilkin, U. Pedersen, A. Foster, N. De

Maio, M. Basham, F. Yuan, K. Wanelik, beamlines I12 : the Joint Engineering , Environment and Processing (JEEP) beamline at Diamond Light Source beamlines, J. Synchrotron Radiation2. 22 (15AD) 828–838.

[39] I. Arganda-carreras, V. Kaynig, C. Rueden, K.W. Eliceiri, J. Schindelin, A. Cardona, H.S. Seung, Trainable Weka Segmentation : a machine learning tool for microscopy pixel classification, Bioinformatics. 33 (2017) 2424–2426.

[40] M. Doube, M.M. Klosowski, I. Arganda-Carreras, F.P. Cordelières, R.P. Dougherty, J.S. Jackson, B. Schmid, J.R. Hutchinson, S.J. Shefelbine, BoneJ: Free and extensible bone image analysis in ImageJ, Bone. 47 (2010) 1076–1079.

[41] M.K. Choudhary, R.M. Potter, Heat transfer in glass-forming melts, in: L.D. Pye, A. Montenero, I. Joseph (Eds.), Prop. Glas. Melts, Second, CRC Press, Taylor & Francis, 2005.

[42] E.W. Lemmon, R.T. Jacobsen, Viscosity and thermal conductivity equations for nitrogen, oxygen, argon, and air, Int. J. Thermophys. 25 (2004) 21–69.

[43] A. Michels, J. V Sengers, P.S. van der Gulik, The thermal conductivity of carbon dioxide in the critical region, Physica. 28 (1962) 1216–1237.

[44] A.A. Proussevitch, D.L. Sahagian, V.A. Kutolin, Stability of foams in silicate melts, J. Volcanoogy Geotherm. Res. 59 (1993) 161–178.

[45] F. Méar, P. Yot, M. Ribes, Effects of temperature, reaction time and reducing agent content on the synthesis of macroporous foam glasses from waste funnel glasses, Mater. Lett. 60 (2006) 929–934.

[46] A. Bhakta, E. Ruckenstein, Decay of standing foams: Drainage, coalescence and collapse, Adv. Colloid Interface Sci. 70 (1997) 1–124.

[47] J. König, V. Nemanič, M. Žumer, R.R. Petersen, M.B. Østergaard, Y. Yue, D. Suvorov, Evaluation of the contributions to the effective thermal conductivity of an open-porous type foam glass, Constr. Build. Mater. 214 (2019) 337–343.

[48] H.W. Russell, Principles of heat flow in porous insulators, J. Am. Ceram. Soc. 18 (1935) 1–5.

[49] R. Landauer, The Electrical Resistance of Binary Metallic Mixtures, J. Appl. Phys. 23 (1952) 779–784.

[50] M. a. Schuetz, L.R. Glicksman, A basic study of heat transfer through foam insulation, J. Cell. Plast. 20 (1984) 114–121.

[51] D.J. Doherty, R. Hurd, G.R. Lestor, The physical properties of rigid polyurethane foams, Chem. Ind. 30 (1962) 1340–1356.

[52] P. Collishaw, J.R.G. Evans, Review An assessment of expressions for the apparent thermal conductivity of cellular materials, J. Mater. Sci. 29 (1994) 2261–2273.

[53] D.S. Smith, A. Alzina, J. Bourret, B. Nait-Ali, F. Pennec, N. Tessier-Doyen, K. Otsu, H. Matsubara, P. Elser, U.T. Gonzenbach, Thermal conductivity of porous materials, J. Mater. Res. 28 (2013) 2260–2272.

[54] Y. Attila, M. Güden, A. Taşdemirci, Foam glass processing using a polishing glass powder residue, Ceram. Int. 39 (2013) 5869–5877.

[55] C. Vancea, I. Lazău, Glass foam from window panes and bottle glass wastes, Cent. Eur. J. Chem. 12 (2014) 804–811.

[56] D.M.A. Alim, Production and characterization of foam glass from container waste glass, The American University in Cairo, 2009.

[57] M.T. Souza, B.G.O. Maia, L.B. Teixeira, K.G. de Oliveira, A.H.B. Teixeira, A.P. Novaes de Oliveira, Glass foams produced from glass bottles and eggshell wastes, Process Saf. Environ. Prot. 111 (2017) 60–64.

[58] L. Van Der Tempel, G.P. Melis, T.C. Brandsma, Thermal conductivity of a glass: I. Measurement by the glass–metal contact, Glas. Phys. Chem. 26 (2000) 606–611.

[59] J. V. Sengers, J.T.R. Watson, Improved International Formulations for the Viscosity and Thermal Conductivity of Water Substance, J. Phys. Chem. Ref. Data. 15 (1986) 1291–1314.

[60] E.S. Udoetok, Thermal conductivity of binary mixtures of gases, Front. Heat Mass Transf. 4 (2013) 1–5.

[61] F. Méar, P. Yot, M. Cambon, M. Ribes, The characterization of waste cathode-ray tube glass, Waste Manag. 26 (2006) 1468–1476.

Graphical abstract